CrossMark

ORIGINAL PAPER

Effect of micro/nano white bamboo fibrils on physical characteristics of epoxy resin reinforced composites

Cuong Manh Vu · Le Hoang Sinh · Hyoung Jin Choi · Tien Duc Pham

Abstract As a green filler comprising both nano- and micro-sized fibrils, micro/nano white bamboo fibrils (MWBFs) were treated with a silane coupling agent (S-MWBFs) prior to their introduction in an epoxy resin (EP). The sequential processes of steam explosion, alkaline treatment, and micro grinding were used to prepare to MWBFs. The effects of the S-MWBFs on various characteristics of the cured EP such as compatibility, fracture toughness, morphology, mechanical property, and flame retardation were studied. The fracture toughness and mechanical characteristics of both the storage modulus and tanδ maximum increased following addition of the S-MWBFs to the EP. Notably, the fracture toughness of the EP with 0.3 wt% of S-MWBFs was 22.2% higher than that of unmodified resin. Scanning electron microscopy presented somewhat rougher surfaces with shear deformation and tortuously twisting cracks, resulting in a higher fracture toughness in S-MWBF-modified epoxy samples. However, fire testing showed that the presence of S-MWBFs increased the burning rate of the EP.

Keywords Epoxy resin · Micro/nano white bamboo fibril · Fracture toughness · Surface morphology · Mechanical property · Silane coupling agent

C. M. Vu
Department for Management of Science and Technology Development, Ton Duc Thang University, Ho Chi Minh, Vietnam

C. M. Vu (✉)
Faculty of Applied Sciences, Ton Duc Thang University, Ho Chi Minh, Vietnam
e-mail: vumanhcuong1@tdt.edu.vn

L. H. Sinh (✉)
Center for Advanced Chemistry, Institute of Research and Development, Duy Tan University, Da Nang, Vietnam
e-mail: lehoangsinh@dtu.edu

H. J. Choi (✉)
Department of Polymer Science and Engineering, Inha University, Incheon 22212, Korea
e-mail: hjchoi@inha.ac.kr

T. D. Pham
Faculty of Chemistry, Hanoi University of Science, Vietnam National University, Hanoi, 19 Le Thanh Tong, Hoan Kiem, Hanoi 10000, Vietnam

Introduction

Epoxy resin (EP) has been regarded as one of the most important organic engineering matrices for fabricating composite materials due to its high modulus of elasticity and strength, low shrinkage during cure, and easy processability (Barbosa et al. 2016; Shin et al. 2017; Kang et al. 2017; Ren et al. 2017). Associated with chemical structure of the EP, epoxy matrix-based composites have been adopted in various industries, such as aerospace, automotive, and marine construction (Heng et al. 2015), and have possessed desirable

physical and mechanical properties, thermal stability, and chemical resistance. However, due to the high crosslink density after curing, epoxy has shown the main disadvantage of being brittle, requiring relatively low energy for its deformation and crack propagation; this feature has limited its use in engineering applications that require high toughness (Li et al. 2016). For this reason, an intermediate phase through blending or chemical modification has been introduced to improve the brittleness problem. Enhancement of the EP toughness can be achieved by elastomers (Vijayan et al. 2015; Quan and Ivankovic 2015), thermoplastics (Liu et al. 2015), or solid particles such as silica (Zhang et al. 2008; Dittanet and Pearson 2013), graphene (Leopold et al. 2016; Hawkins and Haque 2014), graphene oxide (Wan et al. 2014), aluminum beads (Sperandio et al. 2010; Zhao et al. 2008), or core–shell nanoparticles (Liu et al. 2016).

Concurrently, researchers have also investigated renewable and non-petroleum sources as modifiers for EPs due to environmental concerns (Suyanegara et al. 2011; Minelli et al. 2010; Lu et al. 2008; Chiappone et al. 2011; Yang et al. 2011). Cellulose, as one of the most plentiful bio-polymeric substances, can be found in plant cell walls, secretion from bacterial cell walls, and some marine animals. When used as fillers, these fibers enhance the mechanical characteristics of polymer matrices. Therefore, cellulose fibers have become the most attractive re-enforcer for enhancing the material properties of polymers because they have high strength and high modulus but are also environmentally benign, biodegradable, and sustainable with cheap price. Alamri and Low (2012) fabricated recycled cellulose fiber-filled epoxy composite with four different fiber loading up to 46 wt%, showing that best mechanical characteristics were obtained for a fiber content of 46 wt%. Yeo et al. (2017) used microfibrillated cellulose modified with triethoxy(3-glycidylpropyl) silane as the reinforcing filler for EP to improve mechanical characteristics of the epoxy-based composite. Both critical stress intensity factor (K_{IC}) and critical strain energy release rate (G_{IC}) exhibit enhanced interfacial adhesion between the epoxy base and the cellulosic re-enforcer in the triethoxy(3-glycidylpropyl) silane-modified microfibrillated cellulose/epoxy composites and increased fracture toughness. Zhao et al. (2017) used cellulose nanofibers with their surfaces modified with polyethyleneimine to increase mechanical behaviors of EP.

Both tensile strength and Young's modulus of the obtained nanocomposites were 88 and 237%, higher than those of the pristine epoxy, respectively, while their storage modulus was improved a lot at temperatures either below or above the glass transition temperature (T_g). Recently, Saba et al. (2017) investigated the effect of the cellulose nanofiber content on the mechanical characteristics, morphology, and structure of epoxy-based composites. The experimental analysis clearly revealed that 0.75 wt% was the most effective content of cellulose nanofiber filler to obtain the optimum values of both mechanical and structural characteristics of the epoxy-based composites.

Micro-fibrillated cellulose, which has a diameter in the range of 10–100 nm possessing a web-like structure, is obtained from various cellulosic sources using high pressure homogenization, fluidization, grinding, and cryo-crushing (Grabr et al. 2010a, b; Spence et al. 2011; Alila et al. 2013). The Young's modulus and tensile strength of micro-fibrillated cellulose are estimated at 100–140 and 2–3 GPa, respectively. The Young's modulus of micro-fibrillated cellulose is known to be similar to that of a perfect crystalline native cellulose (167.5 GPa) (Lavoine et al. 2012).

Although microfibrillated cellulose has been fabricated from different sources and used as an effective filler for EP, to the best of our knowledge both the fabrication of micro/nano-sized white bamboo fibril (MWBF) from white bamboo and its usage as a filler for EP have been seldom reported. The combined processes of steam explosion, alkaline treatment, and micro grinding to produce the micro/nano cellulose fiber are considered to be new. Furthermore, a slurry state of the fabricated microfibrillated cellulose in water was used as a source of fiber for the EP. This was achieved by applying a solvent exchange method without a drying process, which is a unique approach of this work and differs from all other previously reported strategies (Alamri and Low 2012; Yeo et al. 2017; Zhao et al. 2017; Saba et al. 2017), in which the microfibrillated cellulose (via a dispersion method) was dried before being incorporated into the EP.

The aims of this work are to examine the effect of S-MWBF on fracture toughness, mechanical behaviors, surface morphology, dielectric properties, and flame retardation of EP using methyl hexahydrophthalic anhydride (MHHPA) as a curing agent and 1-methylimidazole (NMI) as an accelerator. The

MWBFs in this study comprised both micro- and nano-sized fibrils and were modified with a silane coupling agent prior to their incorporation into the epoxy resin. Note that dispersion methods are required to achieve good dispersion of fibrils in the EP on the nanoscale.

Experiment and methods

The EP used was the diglycidyl ether of bisphenol A (DGEBA) (Epon 828, Shell Chemical) with an epoxide equivalent weight of 185–192 g/eq. MHHPA (Lindau Chemical, UK) was selected as a curing agent whereas NMI (BASF, Germany) was used as an accelerator. The silane coupling agent (3-glycidyloxypropyl) trimethoxysilane (GS) was purchased from Sigma Aldrich. *Dendrocalamus membranaceus munro* (white bamboo) ($\sim$ 3 years old) from Hoa Binh Province, Viet Nam was used as the micro/nano fiber source. Ethanol and acetone (Tianjin Yongda Chemical Reagent Co.) were used as solvents. The chemical formulas of DGEBA, MHHPA, and NMI are depicted in Fig. 1.

The MWBFs were synthesized from pristine white bamboo via a steam explosion method followed by alkaline treatment and micro-grinding mechanical extraction. Raw white bamboo ($\sim$ 3 years old) was initially cut into bamboo culms 50–60 cm in length by a saw and then placed into an autoclave for 1 h under over-heated steam condition of 175 °C and 0.8 MPa. The over-heated steam was then released quickly over a period of 5 min and this sudden steam release process was cycled 9 times. Subsequently, the samples were continuously immersed in a 2% NaOH solution at 70 °C for 5 h to ensure complete extraction of the cell walls. A roller looser was then applied to extract the slabs into short fibers. In a final step, the samples were washed using fresh water until a neutral pH was obtained and dried completely in an oven for 24 h at 105 °C. The obtained fibers were suspended in water with a fiber concentration of 10 wt%, and then cut into pulp fibers using a food mixer. The pulp-type fibers were cycled 15 times between static grind and rotating grind stones rotating at 1500 rpm (MKCA6-3, Masuko Sangyo, Japan). The obtained aqueous MWBF slurry with 90% water was treated with ethanol to remove the water and filtered using a vacuum pump to produce a sheet-type MWBF. The filtered MWBF sheet was mixed with excess ethanol using a stirrer at 5000 rpm for 15 min. The morphology of MWBF was determined by SEM, as shown in Fig. 2c.

The desired amounts of MWBF (0.1–0.4 wt%, calculated based on EP) were dissolved in acetone containing 2 wt% GS and then agitated using a mechanical stirrer at 4000 rpm for 1 h in an ice bath to ensure that no solvent evaporated. Subsequently, the desired amount of epoxy was put and mixed for 60 min. The mixtures were stirred in a heating bath for 1 h at 45 °C, for 1 h at 75 °C, and for 2 h at 90 °C sequentially. The mixtures were then continuously heated at 90 °C for 4 h in an oven in order to completely remove the solvent. Figure 3 presents the detailed steps of this process.

The estimated amounts of the curing agent and accelerator (mass ratio of EP/MHHPA/NMI = 100/87/2.8) were mixed and then degassed in a chamber under vacuum condition for 15 min. This mixture was agitated for 30 min and then poured into a mold which was preheated and treated by spraying a mold-release agent. The curing step was processed at 130 °C for 1 h and then continued for an additional 1 h at 150 °C in a convection oven.

The K_{IC} of the fabricated samples was determined using a single edge notched beam tester in a three-point bending flexure, in which the three-point bending measurement was proceeded using a universal testing machine (Lloyd 500N, England) following the ASTM D5045-99 test method.

Tensile tests were performed using a dumbbell-typed sample (ASTM D638-91, Type I) via a universal testing machine (Instron model 5582-100KN) at room temperature with an extensional rate of 2 mm/min. The obtained tensile stress–strain curves provided ultimate tensile strength of the maximum stress, ultimate elongation at break, and Young's modulus. The flexural test using an Instron (5582-100KN; ASTM D790-86 test method) with a three-point bend configuration and a sample dimension of $5 \times 10 \times 100$ mm^3 was repeated five times per sample to obtain the average values.

The storage modulus and tanδ curves were measured using a dynamic mechanical analyzer (DMA) (DMA8000; ISO 6721–1). The pristine epoxy and composite samples with a dimension of 50 mm (length) $\times$ 8 mm (width) $\times$ 2 mm (thickness) were examined by three-point bending method for different
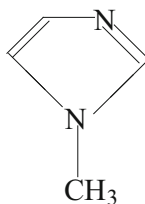
Epoxy resin (EP)
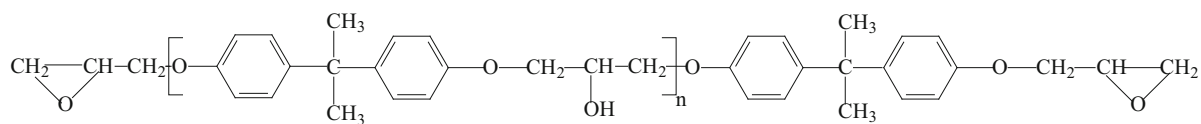
Methyl hexahydrophthalic anhydride (MHHPA)
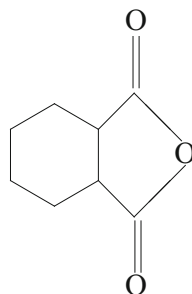
1-Methylimidazole (NMI)

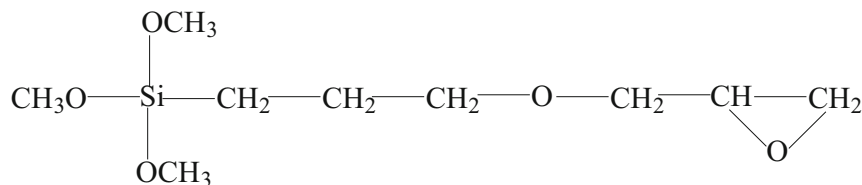(3-Glycidyloxypropyl) trimethoxysilane

Fig. 1 Chemical formulas of the raw materials

temperatures from room temperature to 200 °C at a heating rate of 5 °C/min and a fixed frequency of 6.28 rad/s. The glass transition temperature, T_g, of the composites was obtained from the maximum peak of the tanδ curves. Their fractured surfaces were further

observed by scanning electron microscopy (SEM) (Joel JSM 6360, Japan).

The dielectric constant (ε) and loss tangent value (tanδ) were obtained using a Digital C-Tgδ Meter (mode 0194 C, CEAST) following ASTM D150 at a

Fig. 2 Picture of white bamboo (**a**), prepared MWBF (**b**), and SEM image of MWBF (**c**)
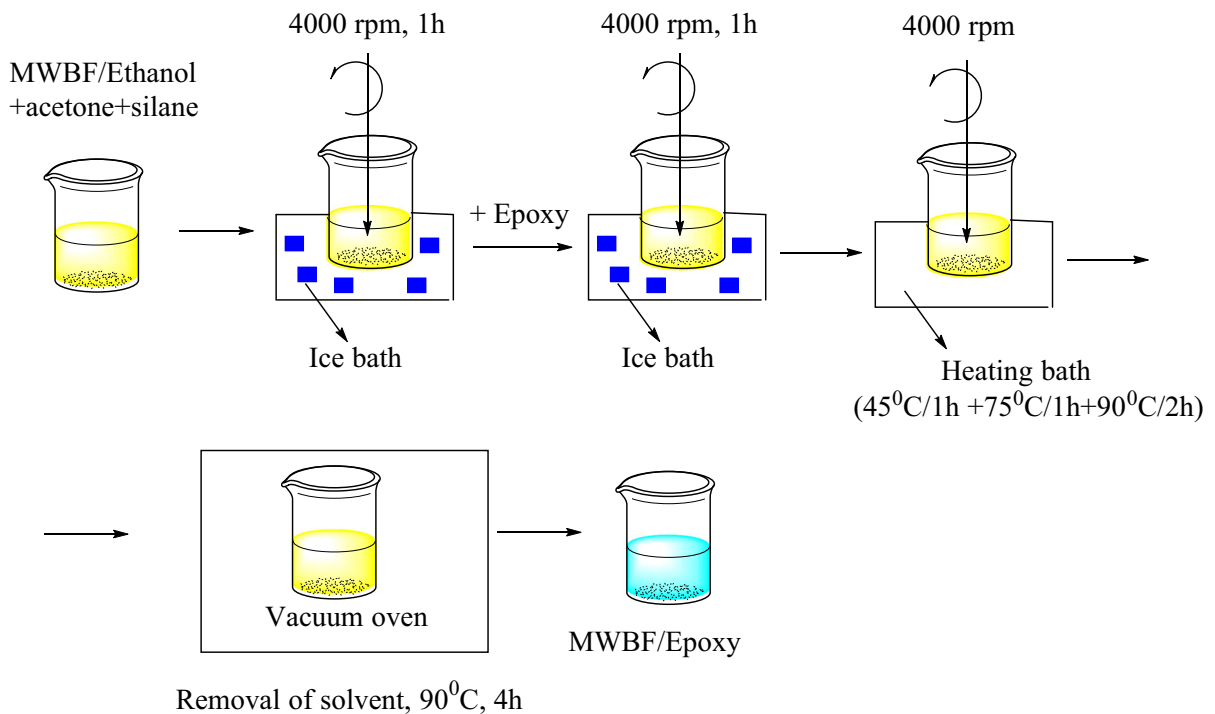

Fig. 3 Fabrication process of EP/MWBF

fixed frequency of 1 MHz. The samples with a dimension of 11 cm in diameter (same size of the capacitor) and < 1 mm in thickness, were prepared from cured epoxy sheets and then inserted between two capacitors. The gap between the two capacitors was tuned to bring the sample as close as possible to record the capacitance (C) and loss tangent. The ε was deduced from the following Eq. (1):

$$C = \epsilon \cdot \epsilon_0 \cdot \frac{A}{d} \tag{1}$$

where C is in Faradays (F), $\epsilon_0 = 8854 \times 10^{-12}$ F/m, A is the overlap area of the two capacitors, and d is the gap between two capacitors, which is equal to the sample thickness (Vu et al. 2016).

The limiting oxygen index (LOI) was tested on an oxygen index meter (FTT, UK) as per ASTM D2863-06 with a sample dimension of $130 \times 6.5 \times 3$ mm^3.

Furthermore, the vertical burning test (UL 94HB test) was carried out using a vertical flame chamber (UL 94, FTT, UK) with a sample size of $125 \times 12.8 \times 3$ mm^3 according to ASTM D635-14.

The samples were stored in a desiccator at 23 °C and relative humidity = 50% for 88 h prior to the test, according to ISO 291. The ignition source was designed according to ASTM D5025 with the flow rate of methane fixed at 105 mm/min. A sample with thickness < 3 mm will reach the condition of UL94HB if the rate of burning is lower than 76 mm/min or the length of the fired part of the sample is < 10 mm. The rate of burning was calculated from at least five samples.

The rate of burning (V) (mm/min) was calculated from the following equation:

$$V = 60 \times \frac{L}{t} \qquad (2)$$

where L is the length of fired sample (mm) and t is time in seconds.

Results and discussion

The morphology of the MWBFs was characterized by SEM, as shown in Fig. 2c. The MWBFs exist in the form of micro-fiber networks with a diameter ranging from 40 to 200 nm and a fiber length greater than 10 μm. Through several treatment steps, the produced white-colored MWBFs were modified with a silane coupling agent and used as a reinforcement material for the EP. Figure 3 shows the modification and dispersion processing of MWBF in EP.

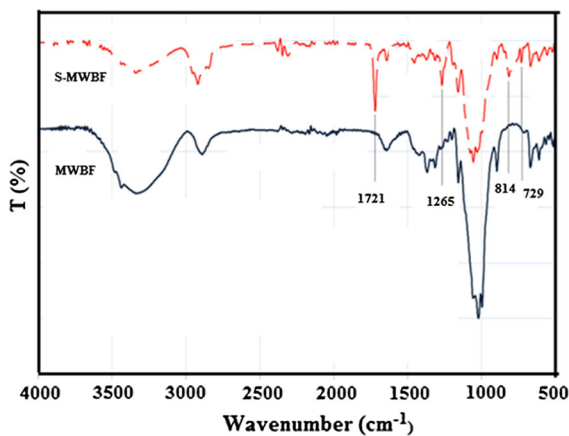Successful silanization of the surface of silane-modified MWBF (S-MWBF) was verified from the

Fig. 4 FTIR spectra of pristine MWBF (solid black line) and MWBF treated with silane S-MWBF (dash red line). (Color figure online)

FTIR analysis, as shown in Fig. 4. The FTIR spectrum of S-MWBF exhibited four new peaks relative to the spectrum of MWBF. The absorption peaks at ∼ 731 and ∼ 1269 cm^{-1} are attributed to stretching and bending vibrations of the C–Si linkage, respectively, which verifies the condensation of silane on the MWBF surface. In addition, the bands detected at 814 and 1721 cm^{-1} in the S-MWBF spectrum are attributed to the epoxy group.

The silanization was further confirmed by elemental analysis (EDX). The EDX spectrum of pristine MWBF shows carbon and oxygen peaks but no silicon peak. After silanization, the EDX spectrum of S-MWBF showed peaks of carbon, oxygen, and silicon, as presented in Fig. 5.

The dispersion and compatibility of micro-fibrils in EP are key factors that can affect the final characteristics of the samples and must consequently be examined. The dispersion of microfibrils in the matrix can provide a measure of the processing effectiveness of the silane-treated microfibrils. The ultimate aims of silane treatment of the microfibrils are the enhancement of compatibility, chemical affinity, and dispersion, and the prevention of fiber aggregation in the base matrix. The compatibility and suspension of nano/micro-fibrils in the EP were directly observed by SEM images after the nano/micro-fibrils were
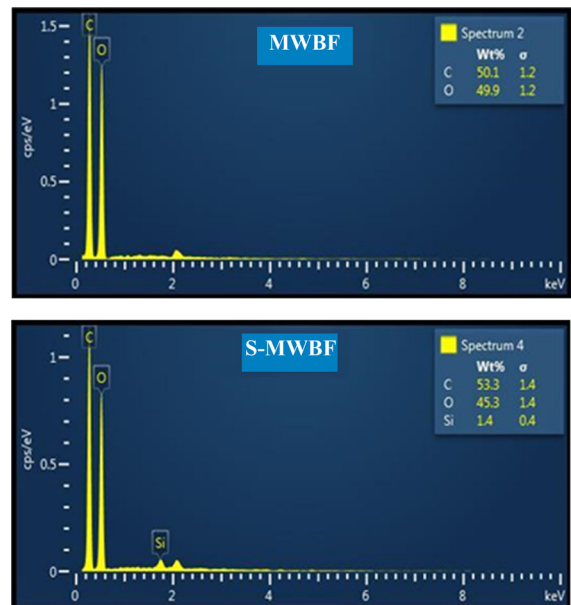

Fig. 5 EDX spectra of pristine MWBF and MWBF treated with silane S-MWBF

dispersed in the uncured EP matrix prior to the curing processing, as shown in Fig. 6.

The SEM images in Fig. 6 show that S-MWBF has good dispersion in the uncured epoxy matrix for all samples with no aggregation and that all microfibrils have been separated from each other as individual single fibers. These results confirm the effectiveness of silane treatment processing on enhancing the fiber surface hydrophobicity. The fracture toughness (K_{IC}) of the resins measured by the single edge notched beam measurement is plotted as a function of filler weight percent (Fig. 7).

As seen in Fig. 7, the fracture toughness increased with increasing S-MWBF in the EP and attained its maximum value at 0.3 wt% S-MWBF. The neat ER was brittle, with a K_{IC} value of 0.63 MPa m$^{1/2}$. In contrast, the S-MWBF-modified EP with 0.3 wt% S-MWBF had the K_{IC} of 0.79 MPa m$^{1/2}$, which is 22% higher than that of the pristine EP. This increase might be due to deflection and pinning process of the crack at the obstacles, which are proposed to play important roles in their toughening mechanism (Zang
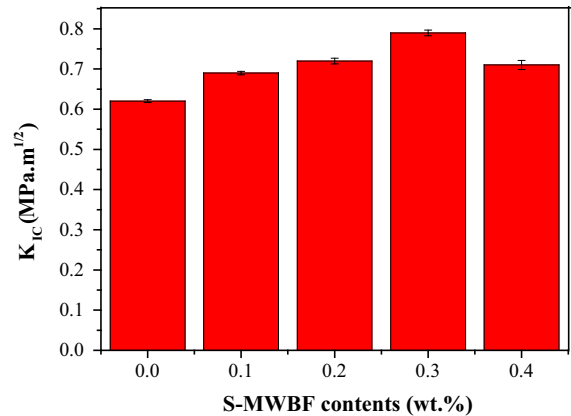

Fig. 7 Toughness values in terms of K_{IC} as a function of S-MWBF content for EP/S-MWBF composites

et al. 2010; Khan and Kim 2012; Gkikas et al. 2012). Better adhesion between the fibers and the EP matrix of the composite due to the presence of GS and to the superior energy-absorbing capability of the fibers suspended in the matrix could cause this improvement. On the other hand, the decreased fracture toughness at
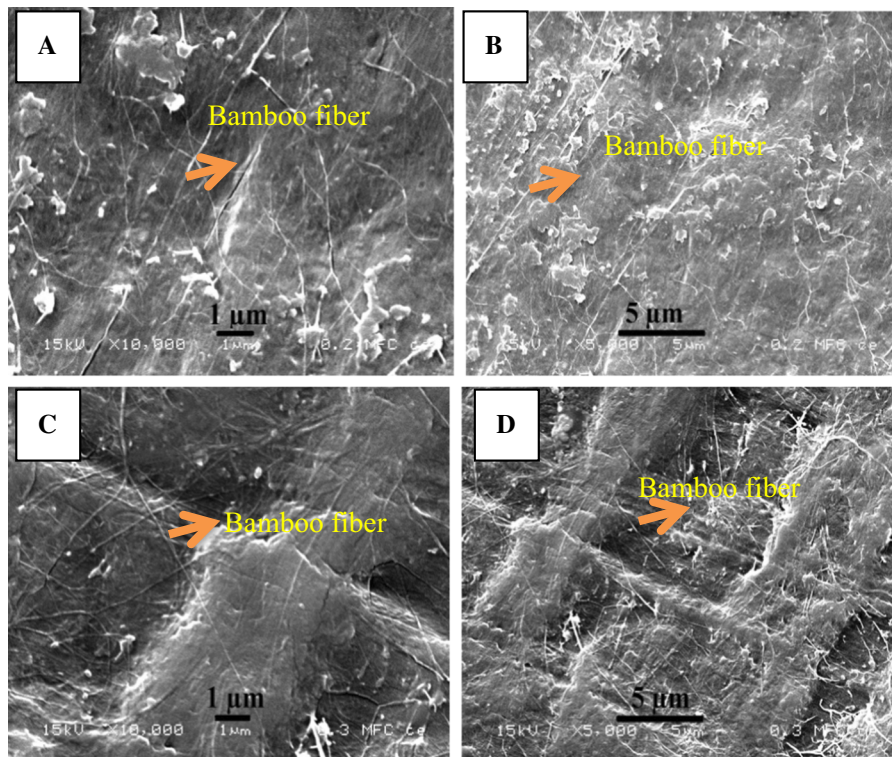

Fig. 6 SEM images of S-MWBF dispersion in the EP matrix with different MWBF contents (**a, b** 0.2 wt% MWBF; and **c, d** 0.3 wt% MWBF)

the higher loading of 0.4 wt% S-MWBF may be caused by S-MWBF aggregation.

Figure 8 presents a schematic representation of the vital role of GS in modifying the fiber surface as well as its incorporation into epoxy matrices.

The GS silane coupling agent with a structural mono oxirane group helped to incorporate MWBF into the epoxy main chain via the curing processing, resulting in an improved fracture toughness.

The mechanical performances of the unmodified EP and S-MWBF-modified EP were evaluated using both flexural and tensile tests. The flexural strength (σ_f) and elastic modulus (E_b) were measured by a three-point bending test and estimated using the following Eqs. (3) and (4) (Jiang et al. 2012; Jin and Park 2008; Park et al. 2004):

$$\sigma_f = \frac{3PL}{2bd^2} \tag{3}$$

$$E_b = \frac{L^3}{4bd^3} \cdot \frac{\Delta P}{\Delta m} \tag{4}$$
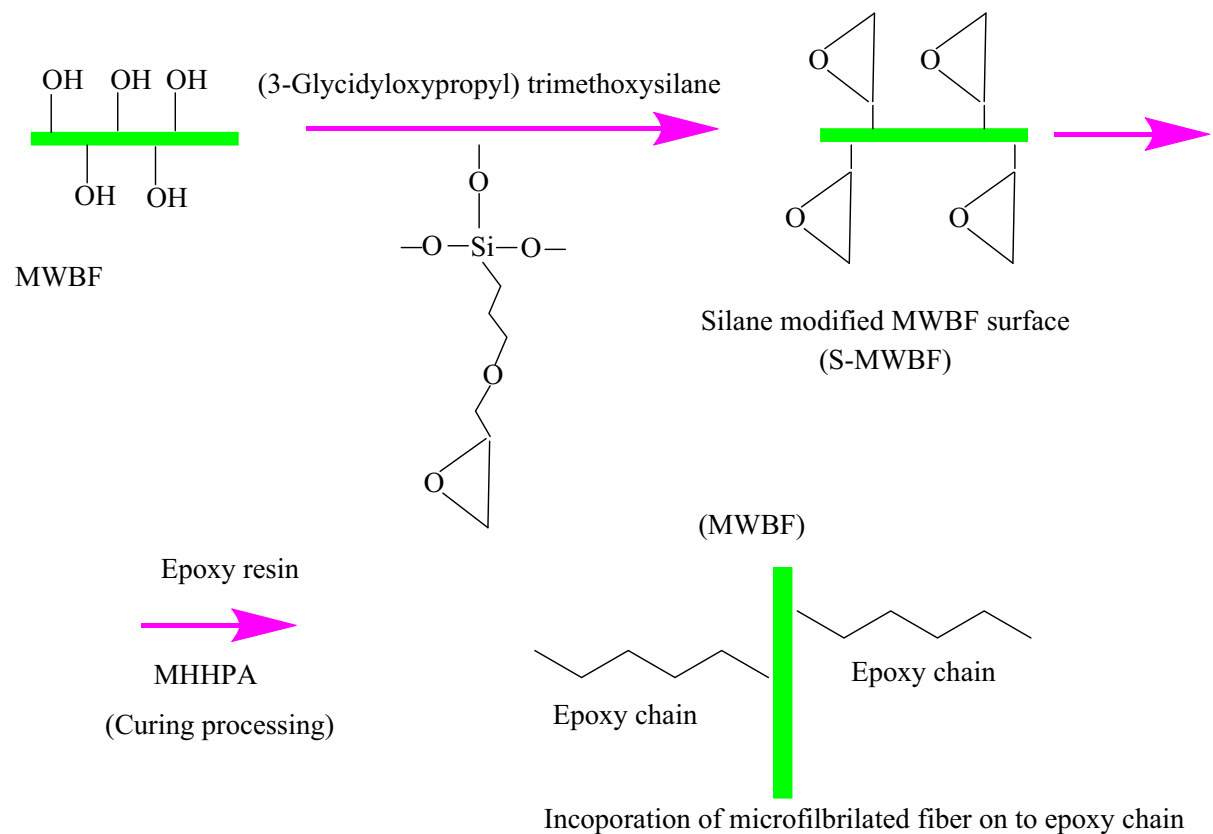
where P is the input load (N), L is the length (mm), b is the sample width (mm), and d is the sample thickness (mm). ΔP is the force change in the linear portion of the load–deflection curve, and Δm is the deflection change corresponding to ΔP.

Table 1 illustrates that the flexural strength (σ_f) and elastic modulus (E_b) of the composites slightly improved with increased S-MWBF content. Their σ_f values increased from 103.7 MPa for neat EP to 112.4 MPa when the S-MWBF content was 0.3 wt% in the composite. These increased flexural strength and elastic modulus might be originated from the increased interfacial bond strength at the fiber-matrix interface.

The effects of S-MWBF on the tensile properties are given in Table 2, and Fig. 9 presents typical tensile stress–strain curves of the EP samples for different S-MWBF contents.

The tensile strength values, tensile moduli, and maximum strains of the composites are improved in the presence of S-MWBF. The slopes of the stress–


Fig. 8 Modification of MWBF surfaces with silane coupling agent and incorporation into the epoxy chain

Table 1 Flexural properties of unmodified EP and EP modified with different S-MWBF contents

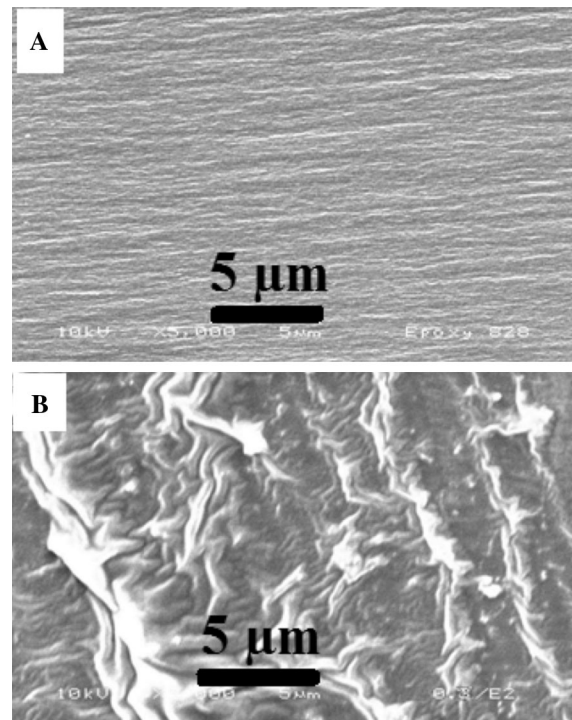| Materials	Flexural strength (MPa)	Elastic modulus (GPa)
Unmodified EP	103.70 ± 0.31	2.050 ± 0.005
EP/0.1 wt% S-MWBF	112.40 ± 0.36	2.110 ± 0.006
EP/0.2 wt% S-MWBF	115.70 ± 0.23	2.330 ± 0.003
EP/0.3 wt% S-MWBF	117.40 ± 0.22	2.410 ± 0.005
EP/0.4 wt% S-MWBF	115.10 ± 0.49	2.130 ± 0.008

Table 2 Tensile properties of unmodified EP and S-MWBF modified-EP

Materials	Tensile strength (MPa)	Tensile modulus (GPa)	Max strain (%)
Unmodified EP	48.22 ± 0.25	0.910 ± 0.007	4.550 ± 0.015
EP/0.1 wt% S-MWBF	54.85 ± 0.58	0.970 ± 0.002	5.210 ± 0.008
EP/0.2 wt% S-MWBF	57.03 ± 0.72	1.120 ± 0.005	5.670 ± 0.011
EP/0.3 wt% S-MWBF	59.81 ± 0.74	1.170 ± 0.009	5.830 ± 0.010
EP/0.4 wt% S-MWBF	54.37 ± 0.49	0.950 ± 0.004	5.470 ± 0.010
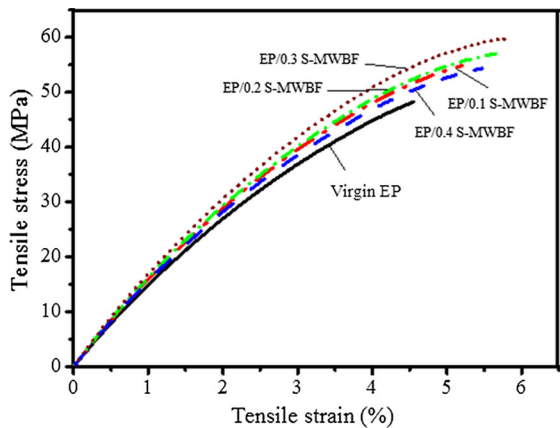
Fig. 9 Tensile stress–strain of unmodified EP (solid black line) and EP/S-MWBF with different S-MWBF contents: 0.1 wt% (dash dot red line), 0.2 wt% (short dash dot green line), 0.3 wt% (short dot brown line), and 0.4 wt% (dash blue line). (Color figure online)

Fig. 10 SEM images of composites after the K_{IC} tests with: **a** pristine epoxy; **b** 0.3 wt% S-MWBF

strain curve appear higher with increased S-MWBF content. The tensile strength, tensile modulus, and maximum strain of the EP/0.3 wt% S-MWBF composite were 7.21, 6.59, and 15.5% higher than those of the pristine cured EP, respectively. Again, these results confirm the strong interfacial bonding between the fiber fillers and the EP matrix. Subsequent to the K_{IC} tests, the fracture surface of the pristine epoxy and EP/0.3 wt% S-MWBF composite was examined using SEM (Fig. 10).

Figure 10a represents that fractured surface of the pristine epoxy matched with a typical brittle fracture property of thermosetting polymers. A smooth and glassy mirror-like surface morphology with micro-flow lines was revealed. In contrast, Fig. 10b shows a rough fractured surface of the modified EP at 0.3 wt% S-MWBF with shear-like stick–slip shapes. Rugged multi-plane patterns appear more prominent than the

neat epoxy surface. For this reason, the S-MWBF-modified epoxy would likely require more energy than that for neat epoxy to cause deformation and/or crack propagation. The toughening result might come from the fact that the matrix cracks faced obstacles of the interfacial fiber bridging, which progressively deflected and changed the crack direction (Grabr et al. 2010a, b; Bortz et al. 2011; Hohnsen et al. 2007; Chen et al. 2012).

The effect of S-MWBF on thermo-mechanical property of the EP was measured using the DMA. DMA test over an extensive temperature range is very sensitive to the physical interactions and chemical structures of the components in polymer composites, allowing study of glass transition or secondary transition and yielding behavior related to the polymer morphology. Results of the dynamic bending tests performed on composites are given in Fig. 11 as a function of temperature from 25 to 200 °C.
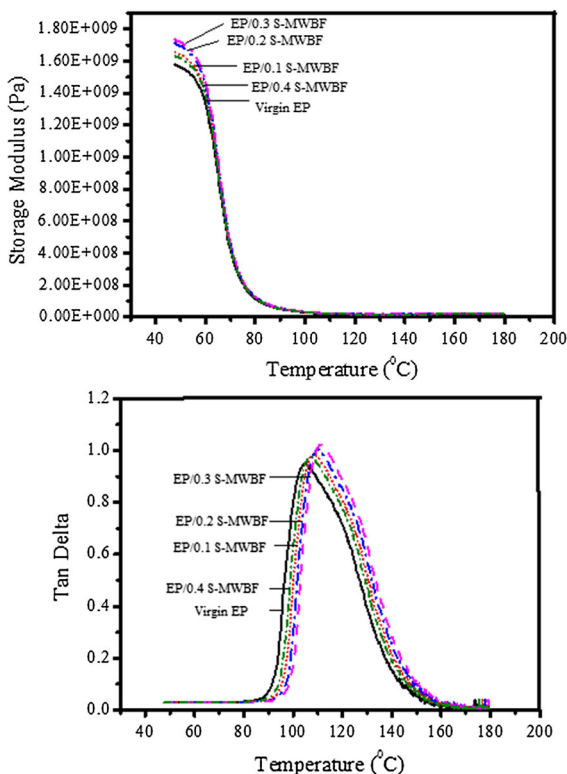
The storage moduli for the composites with different S-MWBF contents are larger than that of the pristine EP, possibly due to the interfacial interaction between the MWBF and EP. The enhanced interfacial interaction caused by MWBF hindered the mobility of the local EP molecular chains around the MWBF.

The tanδ values of the composites were estimated from the ratio of the loss modulus to the corresponding storage modulus measured by the DMA test, as given in Fig. 11. The maximum value of tanδ for the unmodified EP was lower than those of the composites with S-MWBF, possibly due to the fact that adhesion between MWBF and EP supported the energy dissipation from the EP matrix to the MWBF.

Figure 11 also shows that the T_g of the unmodified epoxy resin and composite reinforced with 0.1, 0.2, 0.3, and 0.4 wt% S-MWBF were 104.1, 108.8, 109.4, 111.7, and 107.5 °C, respectively. A slight increase in T_g in the composites with increasing S-MWBF content from 0.1 to 0.3 wt% was observed. However, the T_g decreased at a S-MWBF content of 0.4 wt%. This result may be due to S-MWBF aggregation at higher S-MWBF loadings in the EP.

The ε and tanδ from the dielectric measurement of the unmodified EP and modified EP with 0.1, 0.2, 0.3, and 0.4 wt% MWBF were 2.18, 2.19, 2.23, 2.27, and 2.29, and 0.019, 0.002, 0.021, 0.022, and 0.023, respectively. As seen, there is a slight increasing trend for both the dielectric constant and the loss factor as the S-MWBF content increases. However, these values are small, indicating that the material possesses an external electric field and that there is minimal loss throughout these materials.

LOI and UL94 experiments were conducted to examine effect of the S-MWBF concentration on the flame retardation properties of the EP. The results in Table 3 show that the LOI decreased as the S-MWBF

Fig. 11 Storage modulus and tanδ for unmodified EP (solid black line) and EP composites with S-MWBF: 0.1 wt% (short dot red line), 0.2 wt% (dash dot blue line), 0.3 wt% (dash purple line), and 0.4 wt% (short dash dot olive line). (Color figure online)

Table 3 Flame retardant properties of unmodified EP and S-MWBF-modified EP

Materials	LOI (%)	V (mm/min)
Unmodified EP	21.7	34.3
EP/0.1 wt% S-MWBF	21.1	34.9
EP/0.2 wt% S-MWBF	20.6	35.2
EP/0.3 wt% S-MWBF	20.1	35.8
EP/0.4 wt% S-MWBF	19.4	36.4

content increased. In contrast, the rate of burning of the EP slightly increased in the presence of S-MWBF, demonstrating that MWBF plays a vital role as a flammable component to accelerate burning.

Conclusions

In summary, S-MWBF-reinforced EP composites were fabricated as green composite materials. The fracture toughness, morphological behavior, and mechanical and thermo-mechanical characteristics of neat EP and its composites with varied S-MWBF content (0, 0.1, 0.2, 0.3, and 0.4 wt%) were studied. The addition of S-MWBF increased the flexural strength, flexural modulus, tensile strength, tensile modulus, fracture toughness, and thermal property of the EP. This increase in flexural and tensile moduli by adding S-MWBF demonstrates an improvement in the EP stiffness. Improvement of the fracture toughness was proved from SEM images, which demonstrated that a relatively rougher surface with jagged multi-plane patterns appeared in the S-MWBF-modified epoxy samples, thereby hindering deformation and crack propagation. The DMA test showed a slight increase of the storage modulus and T_g of the EP following addition of S-MWBF. In the presence of S-MWBF, the LOI decreased and the rate of burning increased. The dielectric test showed that S-MWBF had no positive effect on the dielectric constant or loss factor.

References

Alamri H, Low IM (2012) Mechanical properties and water absorption behaviour of recycled cellulose fibre reinforced epoxy composites. Polym Test 31:620–628. doi:10.1016/j.polymertesting.2012.04.002

Alila S, Besbes I, Vilar MR, Mutjé P, Boufi S (2013) Non-woody plants as raw materials for production of microfibrillated cellulose (MFC): a comparative study. Ind Crops Prod 41:250–259. doi:10.1016/j.indcrop.2012.04.028

Barbosa AQ, da Silva LFM, Abenojar J, Figueiredo M, Öchsner A (2016) Toughness of a brittle epoxy resin reinforced with micro cork particles: effect of size, amount and surface treatment. Compos B 114:299–310. doi:10.1016/j.compositesb.2016.10.072

Bortz DR, Merino C, Gullon IM (2011) Carbon nanofibers enhance the fracture toughness and fatigue performance of a structural epoxy system. Compos Sci Technol 71:31–38. doi:10.1016/j.compscitech.2010.09.015

Chen Q, Zhang L, Yoon MK, Wu XF, Arefin RH, Fong H (2012) Preparation and evaluation of nano-epoxy composite resins containing electrospun glass nanofibers. J Appl Polym Sci 124:444–451. doi:10.1002/app.35111

Chiappone A, Nair JR, Gerbaldi C, Jabbour L, Bongiovanni R, Zeno E (2011) Microfibrillated cellulose as reinforcement for Li-ion battery polymer electrolytes with excellent mechanical stability. J Power Sources 196:10280–10288. doi:10.1016/j.jpowsour.2011.07.015

Dittanet P, Pearson RA (2013) Effect of bimodal particle size distributions on the toughening mechanisms in silica nanoparticle filled epoxy resin. Polymer 54:1832–1845. doi:10.1016/j.polymer.2012.12.059

Gkikas G, Barkoula NM, Paipetis AS (2012) Effect of dispersion conditions on the thermo-mechanical and toughness properties of multi walled carbon nanotubes-reinforced epoxy. Compos Part B 43:2697–2705. doi:10.1016/j.compositesb.2012.01.070

Grabr MH, Elrahamn MA, Okubo K, Fujii T (2010a) Effect of microfibrillated cellulose on mechanical properties of plain-woven CFRP reinforced epoxy. Compos Struct 92:1999–2006. doi:10.1016/j.compstruct.2009.12.009

Grabr MH, Elrahamn MA, Okubo K, Fujii T (2010b) Interfacial adhesion improvement of plain woven carbon fiber reinforced epoxy filled with micro-fibrillated cellulose by addition liquid rubber. J Mater Sci 45:3841–3850. doi:10.1007/s10853-010-4439-y

Hawkins DA Jr, Haque A (2014) Fracture toughness of carbon-graphene/epoxy hybrid nanocomposites. Procedia Eng 90:176–181. doi:10.1016/j.proeng.2014.11.833

Heng Z, Chen Y, Zou H, Liang M (2015) Simultaneously enhanced tensile strength and fracture toughness of epoxy resins by a poly(ethylene oxide)-*block*-carboxyl terminated butadiene-acrylonitrile rubber dilock copolymer. RSC Adv 5:42362–42368. doi:10.1039/C5RA05124J

Hohnsen BB, Kinloch AJ, Mohammed RD, Taylor AC, Sprenger S (2007) Toughening mechanisms of nanoparticle-modified epoxy polymers. Polymer 48:530–541. doi:10.1016/j.polymer.2006.11.038

Jiang W, Jin FL, Park SJ (2012) Thermo-mechanical behaviors of epoxy resins reinforced with nano-Al_2O_3 particles. J Ind Eng Chem 18:594–596. doi:10.1016/j.jiec.2011.11.140

Jin FL, Park SJ (2008) Fracture toughness of difunctional epoxy resin/thermally latent initiator system modified with polyesters. J Ind Eng Chem 14:564–567. doi:10.1016/j.jiec.2008.04.003

Kang WS, Rhee KY, Park SJ (2017) Influence of surface energetics of graphene oxide on fracture toughness of epoxy nanocomposites. Compos B 114:175–183. doi:10.1016/j.compositesb.2017.01.032

Khan SU, Kim JK (2012) Improved interlaminar shear properties of multiscale carbon fiber composites with bucky paper interleaves made from carbon nanofibers. Carbon 50:5265–5277. doi:10.1016/j.carbon.2012.07.011

Lavoine N, Desloges I, Dufresne A, Bras J (2012) Microfibrillated cellulose—its barrier properties and applications in cellulosic materials: a review. Carbohydr Polym 90:735–764. doi:10.1016/j.carbpol.2012.05.026

Leopold C, Liebig WV, Wittich H, Fiedler B (2016) Size effect of graphene nanoparticle modified epoxy matrix. Compos Sci Technol 134:217–225. doi:10.1016/j.compscitech. 2016.08.022

Li T, He S, Stin A, Francis LF, Bates FS (2016) Synergistic toughening of epoxy modified by graphene and block copolymer micelles. Macromolecules 49:9507–9520. doi:10.1021/acs.macromol.6b01964

Liu R, Wang J, Li J, Jian X (2015) An investigation of epoxy/thermoplastic blends based on addition of a novel copoly(aryl ether nitrile) containing phthalazinone and biphenyl moieties. Polym Int 64:1786–1793. doi:10.1002/pi.4980

Liu S, Fan X, He C (2016) Improving the fracture toughness of epoxy with nanosilica-rubber core-shell nanoparticles. Compos Sci Technol 125:132–140. doi:10.1016/j. compscitech.2016.01.009

Lu J, Wang T, Drzal LT (2008) Preparation and properties of microfibrillated cellulose polyvinyl alcohol composite materials. Compos Part A Appl Sci Manuf 39:738–746. doi:10.1016/j.compositesa.2008.02.003

Minelli M, Baschetti MG, Doghieri F, Ankerfors M (2010) Investigation of mass transport properties of microfibrillated cellulose (MFC) films. J Memb Sci 358:67–75. doi:10.1016/j.memsci.2010.04.030

Park SJ, Jin FL, Lee JR (2004) Effect of biodegradable epoxidized castor oil on physicochemical and mechanical properties of epoxy resins. Macromol Chem Phys 205:2048–2054. doi:10.1002/macp.200400214

Quan D, Ivankovic A (2015) Effect of core–shell rubber (CSR) nano-particles on mechanical properties and fracture toughness of an epoxy polymer. Polymer 66:16–28. doi:10. 1016/j.polymer.2015.04.002

Ren X, Peng S, Zhang W, Yi C, Fang Y, Hui D (2017) Preparation of adipic acidpolyoxypropylene diamine copolymer and its application for toughening epoxy resins. Compos B 119:32–40. doi:10.1016/j.compositesb.2017.03.019

Saba N, Mohammad F, Pervaiz M, Jawaid M, Alothman OY, Sain M (2017) Mechanical, morphological and structural properties of cellulose nanofibers reinforced epoxy composites. Int J Biol Macromol 97:190–200. doi:10.1016/j. ijbiomac.2017.01.029

Shin H, Kim B, Han JG, Lee MY, Park JK, Cho M (2017) Fracture toughness enhancement of thermoplastic/epoxy blends by the plastic yield of toughening agents: a multiscale analysis. Compos Sci Technol 145:173–180. doi:10. 1016/j.compscitech.2017.03.028

Spence KL, Venditti RA, Rojas OJ, Habibi Y, Pawlak JJ (2011) A comparative study of energy consumption and physical properties of microfibrillated cellulose produced by different processing methods. Cellulose 18:1097–1111. doi:10.1007/s10570-011-9533-z

Sperandio C, Bardon J, Laachachi A, Aubriet H, Ruch D (2010) Influence of plasma surface treatment on bond strength behaviour of an adhesively bonded aluminium-epoxy system. Int J Adhes Adhes 30:720–728. doi:10.1016/j. ijadhadh.2010.07.004

Suyanegara L, Okumura H, Nakagaito AN, Yano H (2011) The synergetic effect of phenylphosphonic acid zinc and microfibrillated cellulose on the injection molding cycle time of PLA composites. Cellulose 18:689–698. doi:10. 1007/s10570-011-9515-1

Vijayan PP, Pionteck J, Thomas S (2015) Volume shrinkage and cure kinetics in carboxyl-terminated poly(butadiene-co-acrylonitrile) (CTBN) modified epoxy/clay nanocomposites. J Macromol Sci A Pure Appl Chem 52:353–359. doi:10.1080/10601325.2015.1018805

Vu CM, Nguyen TV, Nguyen LT, Choi HJ (2016) Fabrication of adduct filled glass fiber/epoxy resin laminate composites and their physical characteristics. Polym Bull 73:1373. doi:10.1007/s00289-015-1553-7

Wan YJ, Tang LC, Gong LX, Yan D, Li YB, Wu LB, Jiang JX, Lai GQ (2014) Grafting of epoxy chains onto graphene oxide for epoxy composites with improved mechanical and thermal properties. Carbon 69:467–480. doi:10.1016/j. carbon.2013.12.050

Yang HS, Gardner DJ, Nader JW (2011) Characteristic impact resistance model analysis of cellulose nanofibril-filled polypropylene composites. Compos Part A Appl Sci Manuf 42:2028–2035. doi:10.1016/j.compositesa.2011.09.009

Yeo JS, Kim OY, Hwang SH (2017) The effect of chemical surface treatment on the fracture toughness of microfibrillated cellulose reinforced epoxy composites. J Ind Eng Chem 45:301–306. doi:10.1016/j.jiec.2016.09.039

Zang G, Kocsis JK, Zou J (2010) Synergetic effect of carbon nanofibers and short carbon fibers on the mechanical and fracture properties of epoxy resin. Carbon 48:4289–4300. doi:10.1016/j.carbon.2010.07.040

Zhang H, Tang LC, Zhang Z, Friedrich K, Sprenger S (2008) Fracture behaviours of in situ silica nanoparticle-filled epoxy at different temperatures. Polymer 49:3816–3825. doi:10.1016/j.polymer.2008.06.040

Zhao S, Schadler LS, Hillborg H, Auletta T (2008) Improvements and mechanisms of fracture and fatigue properties of well-dispersed alumina/epoxy nanocomposites. Compos Sci Technol 68:2976–2982. doi:10.1016/j.compscitech. 2008.07.010

Zhao J, Li Q, Zhang X, Xiao M, Zhang W, Lu C (2017) Grafting of polyethylenimine onto cellulose nanofibers for interfacial enhancement in their epoxy nanocomposites. Carbohydr Polym 157:1419–1425. doi:10.1016/j.carbpol.2016. 11.025